Nano Energy 91 (2022) 106657

Contents lists available at ScienceDirect

Nano Energy

journal homepage: www.elsevier.com/locate/nanoen

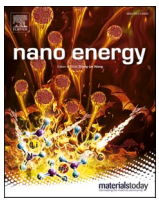

Enhanced Kevlar-based triboelectric nanogenerator with anti-impact and sensing performance towards wireless alarm system

Wenhui Wang [a], Jianyu Zhou [a], Sheng Wang [a,*], Fang Yuan [a], Shuai Liu [a], Junshuo Zhang [a], Xinglong Gong [a,b,**]

[a] CAS Key Laboratory of Mechanical Behavior and Design of Materials, Department of Modern Mechanics, University of Science and Technology of China, Hefei, Anhui 230027, PR China

[b] Frontiers Science Center for Planetery Exploration and Emerging Technologies, University of Science and Technology of China, Hefei, Anhui 230026, PR China

ARTICLE INFO

Keywords:
Triboelectric nanogenerator
Kevlar
Shear thickening composite
Wearable electronics
Bluetooth transmission

ABSTRACT

An enhanced Kevlar-based triboelectric nanogenerator (EK-TENG) with excellent safeguarding and stable sensing capability in harsh loading environments was developed by integrating shear thickening materials and graphene on Kevlar fabric. EK-TENG, whose maximum peak power density reached as high as 25.8 mW/m^2 under oscillator loadings of 40 N and 10 Hz, could directly power commercial LEDs, capacitors and supercapacitors. In addition, the 30-layer EK-TENG with the greatest fiber friction dissipated drop hammer impact force from 1820 N to 439 N under low-speed impact. EK-TENG with anti-ballistic property enabled to resist 126.6 m/s bullet shooting which was higher than 90.1 m/s of neat Kevlar. Besides, EK-TENG effectively absorbed and dissipated 87.4% of the explosion wave energy under blast loading which exhibited excellent safeguarding properties. Furthermore, EK-TENG could generate voltage signals under various impact loadings which could act as self-powered sensor to monitor external stimuli. Finally, a smart TENG-based wireless passive sensor alarm system with high sensitivity was designed to monitor and warn impact dangers, which opened up a new avenue for the development of next generation intelligent protective clothing.

1. Introduction

Smart wearable electronic systems containing signal perception and recognition, data processing, data transmission, reception and reprocessing show wide applications in e-skin, human-machine interaction and smart robots [1–3]. Precisely detecting and sensing various external stimuli was the chief premise for the normal operation of these systems. Particularly, based on triboelectrification and electrostatic induction [4,5], triboelectric nanogenerator (TENG), as a self-powered sensor device with high sensitivity, has shown favorable advantages in smart electronics due to its wide material availability, high efficiency, and flexible usage [6,7]. To further improve the wearability and comfort, various fabric-based TENGs have been designed so far. A TENG-based intelligent shoe with the properties of power supply and human motion monitoring was designed [8]. It also alarmed and rescued remote emergency by wireless signal transmission. Additionally, elastic multifunctional fiber with the energy-harvesting property from body motion was presented which could be served as self-powered tactile sensors for wireless music controllers and human-machine interfaces [9]. Nevertheless, traditional fiber-based TENGs with weak mechanical performance are easily damaged under harsh impact loadings, resulting in structure destruction and electrical performance degradation [10–12]. Consequently, it is necessary to develop novel fiber-based TENG with enhanced anti-impact performance which could be used for intelligent protective clothing.

Kevlar with tensile modulus of 83 GPa, low density and high flexibility enabled to act as an important protective material and has been widely applied in soft body armors [13–15]. They were also used in wearable TENGs. An intelligent protective textile based on graphene/Kevlar showed self-powered monitoring physiological movements and hazard gases properties [16]. Beside good thermal management and self-powered sensing properties, a personal wearable Kevlar device could also resist low-velocity impact loadings [17]. However, the mechanical properties of current developed Kevlar-based TENG were also limited because they only resisted low-speed impact excitation. They

* Corresponding author.
** Corresponding author at: CAS Key Laboratory of Mechanical Behavior and Design of Materials, Department of Modern Mechanics, University of Science and Technology of China, Hefei, Anhui 230027, PR China.
E-mail addresses: wsh160@ustc.edu.cn (S. Wang), gongxl@ustc.edu.cn (X. Gong).

https://doi.org/10.1016/j.nanoen.2021.106657
Received 1 September 2021; Received in revised form 7 October 2021; Accepted 21 October 2021
Available online 28 October 2021

were also destroyed under high speed shock which limited practical application. Besides, previous Kevlar-TENGs only detect external stimuli by outputting voltage signals but the based system with Bluetooth transmission and signal processing property have not been reported yet. To this end, developing Kevlar-TENGs with enhanced mechanical and signal-transmitting properties was urgent for further demand.

Recently, there was a successful strategy to improve the mechanical properties of Kevlar by introducing polymer composites on the fabric [18,19]. Especially, it has been proven that shear thickening materials with rate-dependent mechanical property could significantly enhance the fiber frictions as well as anti-impact performance of the composites [20,21]. Shear thickening materials contain shear thickening fluid (STF) and shear stiffening gel (SSG). The viscosity of non-Newtonian STF can dramatically increase when the shear rate exceeds a critical value and recover immediately after unloading the applied shear rate [22,23]. STF can dissipate impact energy and it has been extensively applied in various areas including anti-impact and damping [24,25]. It was found that the yarn pull-out force of Kevlar fabrics treated with graphene oxide and carbon nanotubes multi-phase STF was almost 2 times that neat Kevlar [26]. Additionally, when Kevlar fabric contains 34.89 wt% STF (STKF), the stab resistance of the 8 layers of STKF was enhanced remarkably than that of 10 layers of neat Kevlar fabric [27]. Moreover, SSG, a derivative of polyborosiloxane, is a soft polymer, which shows a shear stiffening effect similar to STF [28,29]. Its storage modulus increases 3–4 orders of magnitude with the increase of shear frequency [30]. Importantly, the solid SSG is favorable to protect STF from moisture and heat. By combining Kevlar with shear stiffening polymers, the penetration impact energy of composite represented a 50% increment with neat Kevlar [31]. Thus, combining shear thickening materials with Kevlar fiber may develop an impact-resistant TENG and the based

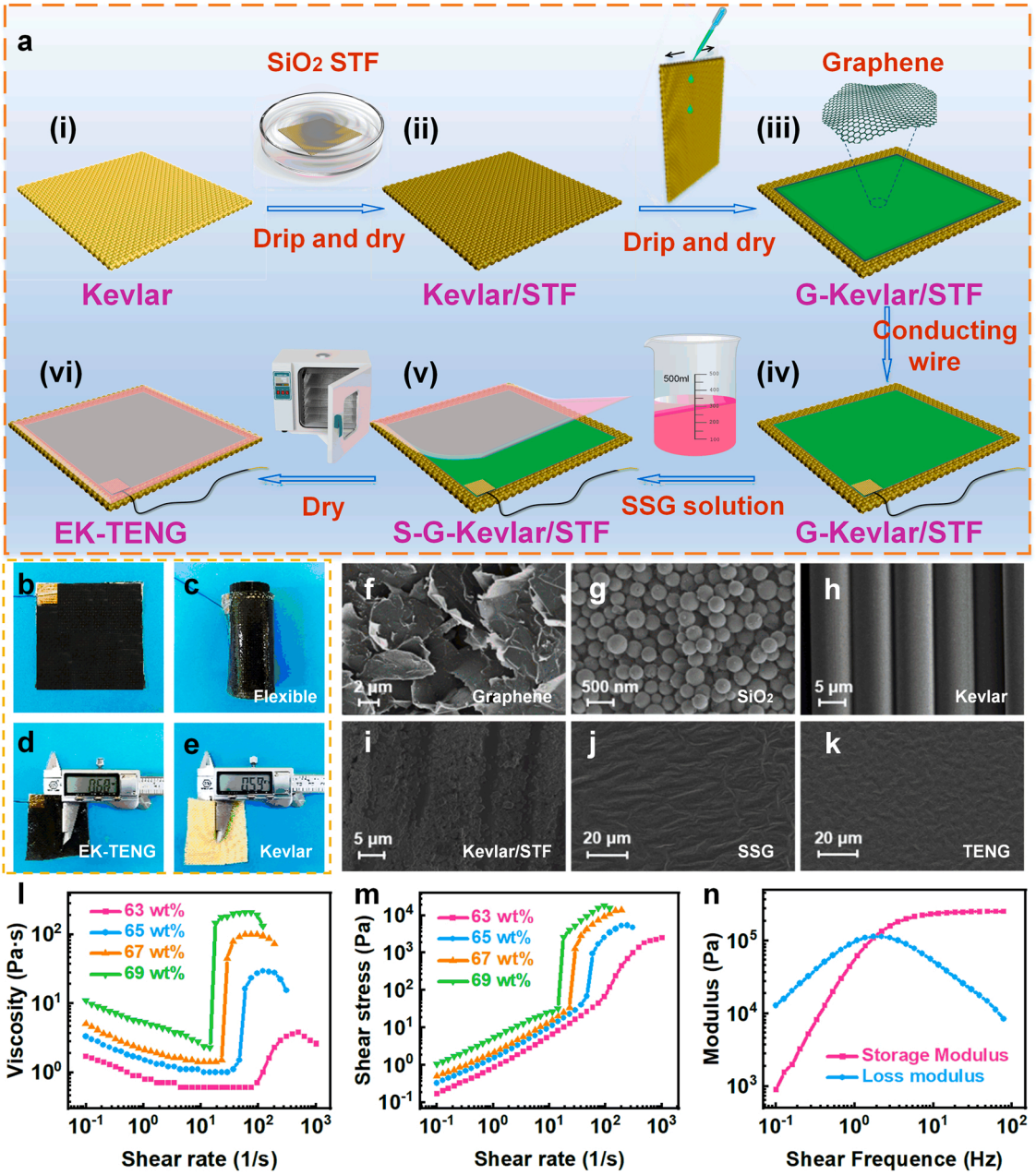

Fig. 1. (a) Fabrication schematic of EK-TENG. (b, c) Photographs of the as-prepared flexible EK-TENG. The thickness of (d) EK-TENG and (e) Kevlar. SEM micrographs of (f) graphene, (g) SiO_2, (h) neat Kevlar, (i) Kevlar/STF, (j) SSG and (k) EK-TENG. Typical rheological properties of STFs: (l) the viscosity and (m) the shear stress vs. shear rate. (n) Storage modulus and loss modulus vs. shear frequency of SSG.

wearable electronic system to realize the perception, transmission and alarm of a variety of external stimuli.

Herein, an enhanced Kevlar-based triboelectric nanogenerator (EK-TENG) with favorable anti-impact and stable self-powered sensing ability during high-speed and high-frequency loading environments was fabricated by introducing STF, graphene and SSG on Kevlar fabric. EK-TENG showed good energy harvesting performance. Owing to the introduction of shear thickening materials, the friction between fibers were dramatically increased. Furthermore, excellent mechanical energy-absorbing performance and stable output voltage signals of EK-TENG were investigated by drop hammer impact test, ballistic impact test, and explosion damage experiment. Finally, a smart TENG-based wireless passive sensor alarm system was designed, which could sense and warn various external impact dangers.

2. Results and discussion

2.1. Preparation and characterization of the composites

The fabrication procedures of EK-TENG were illustrated in Fig. 1a. Briefly, Kevlar fabric (Fig. 1a (i)) was immersed in the SiO_2-based STF to obtain the Kevlar/STF (Fig. 1a (ii)). Then the graphene-ethanol mixture was dripped on the surface of the Kevlar/STF (Fig. 1a (iii)). After attaching a conductive wire on graphene layer (Fig. 1a (iv)), the SSG solution was deposited to form a thin film (Fig. 1a (v)). Finally, EK-TENG was obtained by drying the composites in ovens (Fig. 1a (vi)).

The as-prepared EK-TENG was soft and flexible (Fig. 1b, c) and its thickness increment (0.68 mm) was slight when compared with neat Kevlar (0.59 mm) (Fig. d, e). Furthermore, the SEM image in Fig. 1f displayed the lightweight graphene which was used as an electrode for electrostatic induction and collecting the triboelectric surface charge had a few-layer sheet structure. The silica particles were spherical with an average particle size of 385 nm (Fig. 1g). The surface of neat Kevlar fibers was smooth (Fig. 1h). However, after being treated by STF, the surface of Kevlar/STF and the spaces between fabric yarns were filled with SiO_2 particles (Fig. 1i). Moreover, Fig. 1j and 1k displayed the surface microstructures of the SSG and EK-TENG. The final surface of the EK-TENG was completed covered by insulating SSG.

The as-prepared STF was firstly investigated. SiO_2 contents showed negative influence on the fluidity of STF (Fig. S1). For instance, 63 wt% STF was dilute liquid while 71 wt% STF was in solid state. The rheological properties of the composites were also studied. Fig. 1l and m depicted the typical rheological curves of STFs. As the mass fraction of SiO_2 increased from 63% to 69%, the critical shear rate decreased from 94.3 s^{-1} to 14.3 s^{-1}, the maximum viscosity increased from 3.8 Pa•s to 210.4 Pa•s, respectively. The shear stresses increased slowly with the shear rates, whose slopes increased sharply at the critical shear rates showing the discontinuous shear thickening effect. Based on lower initial viscosity and lighter STF, the STF with 67% mass fraction was selected for further preparation of the EK-TENG in this work. On the other hand, SSG also exhibited typical shear stiffening behavior (Fig. 1n). When the shear frequency was 0.1 Hz, the initial storage modulus (G'_{min}) was 892 Pa, presenting a soft state. As soon as the shear frequency reached 100 Hz, the maximum storage modulus (G'_{max}) increased to 256 kPa. Thus, the shear thickening materials all exhibited rate dependent mechanical properties.

2.2. Triboelectric performance and energy harvesting of the EK-TENG

Fig. 2a demonstrated a schematic illustration of the working mechanism of the EK-TENG. The triboelectric transducing mechanism was dependent on the coupling effect of triboelectrification and electrostatic induction. In the original state, the Poly(methylmethacrylate) plate (PMMA) and EK-TENG were separated away. Electrons transferred from the interface of PMMA to EK-TENG due to their different electron affinity when contacted, resulting in negative triboelectric charges on EK-TENG and positive ones on PMMA (Fig. 2a (i)). As the PMMA left away, there was a potential difference between the two surfaces, leading to the free electrons flow from the electrode to the ground (Fig. 2a (ii)). The system reached electrostatic equilibrium when the PMMA was separated

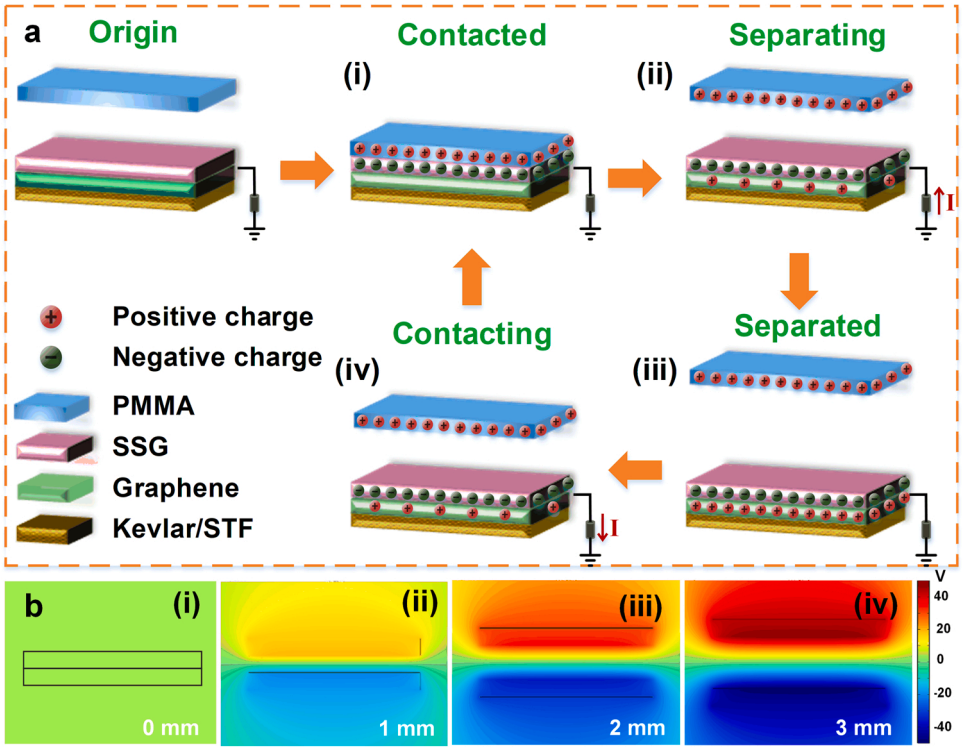

Fig. 2. (a) The working mechanism of EK-TENG. (b) The numerical calculations of the electric potential distribution of EK-TENG between contacting interfaces by COMSOL software.

far away (Fig. 2a (iii)). Conversely, an opposite directional current was generated when the PMMA approached again until the system reversed to the initial state (Fig. 2a (iv)). Besides, the corresponding potential distributions during contact-separation process were simulated by the COMSOL software (Fig. 2b).

The triboelectric properties of EK-TENG were measured by an oscillator system (Fig. S2a). Initially, the influence of loading amplitudes and frequencies on triboelectric properties was investigated. Fig. 3a and Fig. S2b demonstrated the output voltages and currents of EK-TENG with a size of 5 × 5 cm^2 under different applied forces at loading frequency of 10 Hz, respectively. The electric signals showed an increasing trend with the increase of forces. This increment was mainly observed due to the increase in the contact area between the EK-TENG and PMMA. The large deformation of EK-TENG under high pressure led to the number of transferred electrons increased. According to Ohm's law, $U = I \times R = \frac{dQ}{dt} \times R$, where U was output voltage, I was current, R was external resistance and a fixed value, Q was the number of transferred electrons and t was time. Therefore, in the same time, the more charge was transferred, the greater the current, resulting in a high output voltage of EK-TENG. Subsequently, the corresponding voltage signals of EK-TENG at varying input frequencies were presented in Fig. 3b, showing a similar increasing trend. Such an increment was associated due to the decreased separation time and more generated charges accumulated on the electrode. Additionally, the maximum voltage, current and power density of EK-TENG (Fig. 3c) were obtained by varying the external resistance load at 40 N impact force and 10 Hz frequency. When the external resistance increased from 10 kΩ to 1 GΩ, the voltage increased from 57 mV to 45 V, while the current decreased from 5.7 μA to 0.04 μA. The maximum peak power density reached 25.8 mW/m^2 at 10 MΩ. As illustrated in Fig. 3d–f, the EK-TENG showed excellent electrical stability during 1000 cycles of loading-unloading excitations.

Therefore, as a power source, the EK-TENG could effectively output power to light up LED arrays (Fig. S2c). It also enabled to charge commercial capacitors via a rectifier circuit (Fig. S2d). The voltages of smaller capacitance increased faster and the 0.22 μF capacitor exhibited the highest charging voltage of 6.9 V within 15 s (Fig. 3g). In particular, Fig. S2e showed the 3 times of charge-discharge processes of 0.47 μF capacitor were very stable, demonstrating the high reliability of cyclic charging properties. Additionally, a commercial available supercapacitor (SC) was also utilized. The electrochemical properties of SC were investigated by cyclic voltammetry (CV) (Fig. S3a), galvanostatic charge/discharge (GCD) (Fig. S3b) and electrochemical impedance spectroscopy (EIS) (Fig. S3c) measurements using a CHI 760E electrochemical workstation. The shapes of CV loops of SC were close to rectangular even at high scan rates, indicating low contact resistance. The

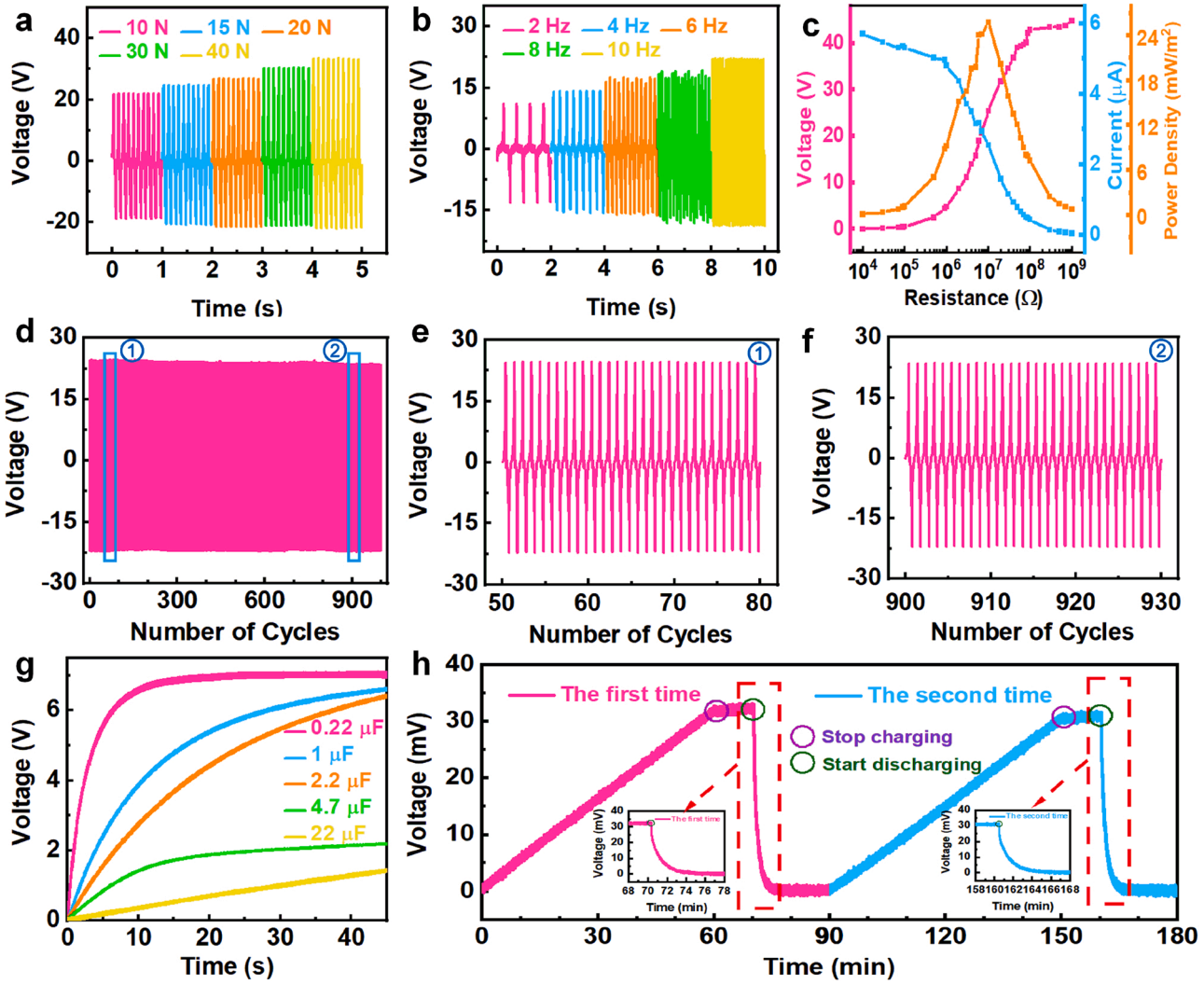

Fig. 3. (a) Force-dependent output voltages at 10 Hz. (b) Frequency-dependent output voltages at 10 N. (c) Voltage, current, and output power under various external resistances. (d–f) Cycling stability of EK-TENG at 10 MΩ. (g) Voltage charging curves of capacitors with different capacitances. (h) The twice charge-discharge curves of supercapacitors at 40 N and 10 Hz.

GCD curves exhibited symmetric triangular shape in all applied current densities, exhibiting the reversible capacitive performance of SC. EIS illustrated the overall resistance of SC was 28 Ω. The charging-discharging processes of SC by EK-TENG were presented in Fig. 3h. It could be directly charged to 33 mV within 60 min and kept stable even stopping charging. When the SC connected to electronics, the process of rapid discharge occurred. Similarly, the voltage of SC reached 25 mV during another charge-discharge process at a smaller loading force (Fig. S3d). Consequently, the as-designed EK-TENG could generate a triboelectric response to external excitation and be used as a power supply device for the capacitors and commercial LEDs.

2.3. Mechanical properties of EK-TENG under yarn pull-out test and drop hammer impact

Since Kevlar was usually used in the field of security protection, it was necessary to study the mechanical properties of EK-TENG. Firstly, the yarn pull-out test was conducted to characterize the fiber friction. As shown in Fig. 4a, the yarn in the middle of the fabrics (38 × 60 mm^2) was used as the pull-out end with the velocities of 0.1, 0.5, 1, 2 and 5 mm/s, respectively. For the neat Kevlar, the pull-out forces were low and the peak pull-out forces (F_{pmax}) fluctuated around 2.0 N which was nearly independent of the pull speed (V_p) (Fig. 4b). Nevertheless, the pull-out forces of Kevlar/STF were significantly improved (Fig. 4c). Besides, the F_{pmax} of EK-TENG showed a similar increasing trend with the increase of V_p (Fig. 4d). As a result, these speed-dependent forces were graphically compared in Fig. 4e. The F_{pmax} value of neat Kevlar was only 2.3 N at the pull-out velocity of 0.1 mm/s, while the F_{pmax} of Kevlar/STF and EK-TENG reached 14.9 N and 17.6 N, respectively. However, at the pull-out velocity of 5 mm/s, the F_{pmax} values of Kevlar/STF and EK-TENG were 26.5 N and 26.9 N, respectively, which were about 14 times as large as Kevlar. Accordingly, the enhancement of the friction force could be attributed to the introduction of STF and SSG. The influence of the STF played a major role in enhancing friction at all pull-out speeds.

Furthermore, the safeguarding and energy-absorbing properties of EK-TENG under low-velocity impact were also investigated. As schematically demonstrated in Fig. S4a, the drop hammer test device was applied to measure the force signals on the back of the composite during the impact process. The drop hammer (0.54 kg) with a sphere indenter (diameter of 20 mm) was released freely from different heights. The impact force at the falling height of 100 mm was presented in Fig. 4f. As the drop hammer directly stroked on the force sensor without a protective layer, the force increased sharply to a maximum value of 1820 N and decayed to 0 within 0.9 ms. However, the maximum force (F_{max}) of the 30-layer Kevlar was 920 N and the buffer time of impact force (Δt) was 1.8 ms. Under the same conditions, the maximum impact force loaded on 30-layer EK-TENG was reduced to 439 N, which reduced by 52.3% compared with neat Kevlar. The buffer time of pedestal, neat Kevlar and EK-TENG were 0.9 ms, 1.8 ms and 2.3 ms, respectively.

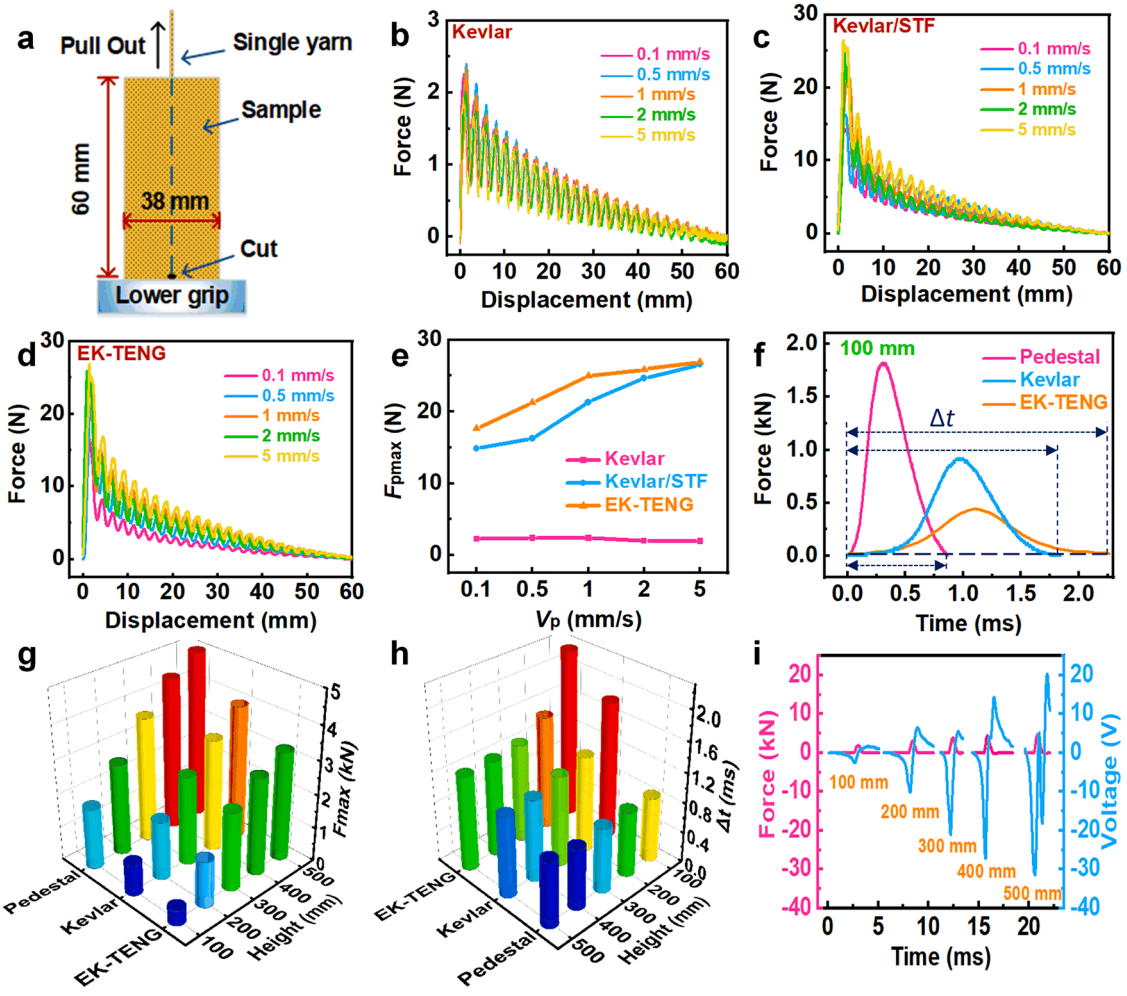

Fig. 4. (a) Yarn pull-out test system. Pull-out force vs. displacement at different pull-out speeds for (b) neat Kevlar, (c) Kevlar/STF, (d) EK-TENG and (e) the maximum force comparison. (f) Typical impact forces of 30-layer Kevlar or 30-layer EK-TENG vs. time loaded by drop hammer falling from 100 mm. Falling height dependent (g) impact force and (h) impact time. (i) The impact force and voltage vs. time with impactor dropping from 100 to 500 mm.

Besides, EK-TENG also showed better force dissipation property under the impact from 200 to 500 mm (Fig. S4b–e). In addition, F_{max} and Δt of all fabrics from different heights were presented in Fig. 4g and h, respectively. There was an increment in F_{max} and a decrement in Δt as the falling height increased. Undoubtedly, at all dropping heights, F_{max} value of EK-TENG was smaller whereas the value of Δt of EK-TENG was longer than other fabrics. So, introducing shear thickening materials into Kevlar was an effective strategy to improve the mechanical properties of the fiber composite which EK-TENG showed better safeguarding performance under impact conditions. On the other hand, EK-TENG could output voltage signals owing to the self-powered sensing effect (Fig. 4i). The negative peak voltage showed an increasing trend with the increase in dropping heights. For example, the voltages falling from 100 to 500 mm were −2.4 V, −10.1 V, −20.9 V, −27.1 V and −31.5 V, respectively. This indicated the output voltages could be used to assess external impact forces. In conclusion, the EK-TENG not only showed favorable anti-impact properties but also presented self-powered force sensing performance under low-speed impact.

2.4. EK-TENG protection and sensing characteristics under ballistic impact

Additionally, the anti-impact protection property of EK-TENG was further investigated under high-speed impact. The ballistic impact experiments were conducted by using a gas gun to drive a spherical bullet (mass of 2 g, diameter of 8 mm) with different initial velocities

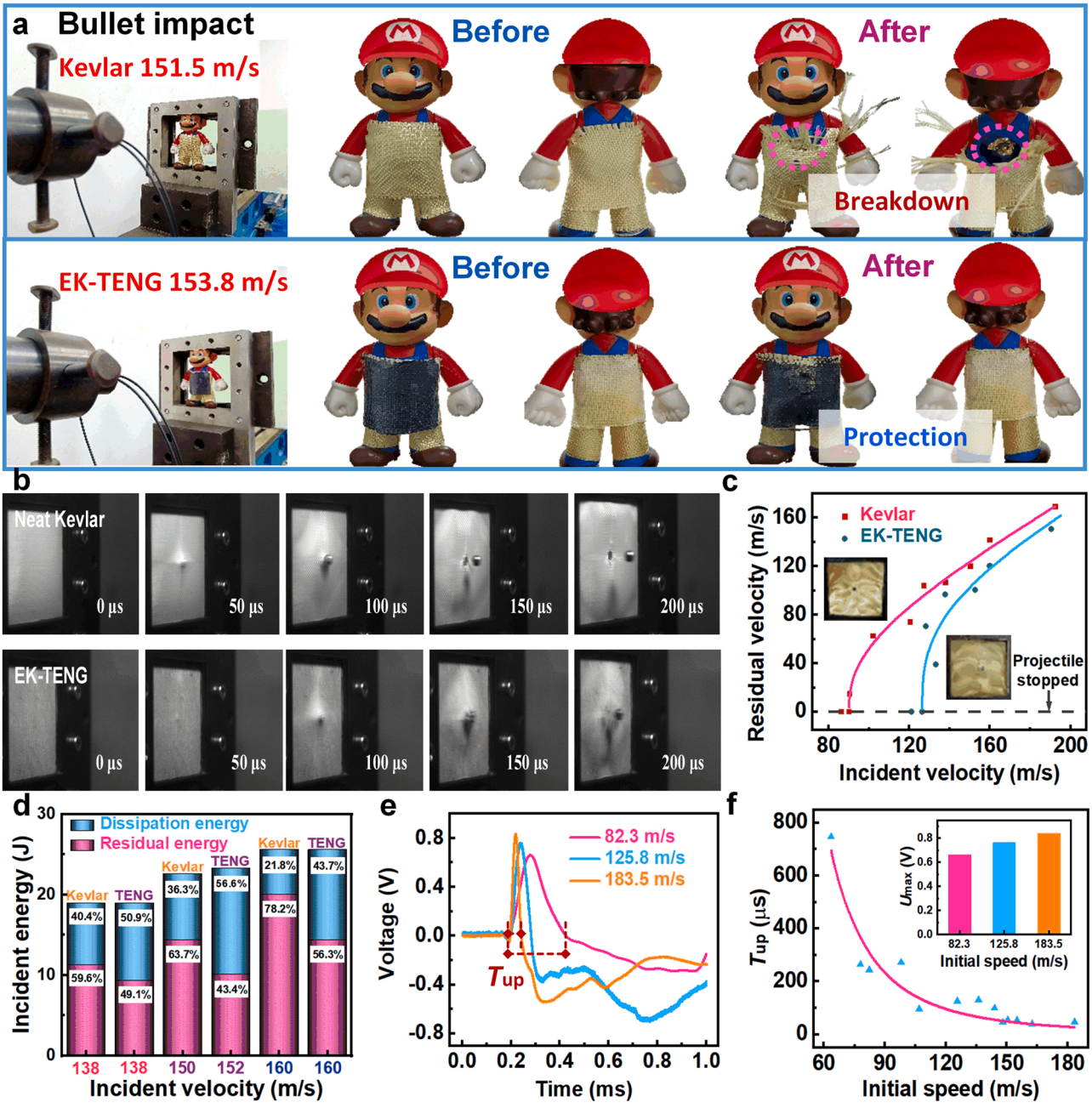

Fig. 5. (a) The scenario of safeguarding properties of EK-TENG-based suit under high speed shooting. (b) The impact process of neat Kevlar and EK-TENG with an incident velocity of 160 m/s. (c) The residual velocity of neat Kevlar and EK-TENG under various impacts. (d) The energy dissipation ratios of Kevlar and EK-TENG under impact excitation. (e) Voltage signals of EK-TENG generated by the bullet impacts with 82.3, 125.8 and 183.5 m/s. (f) Impact velocity-dependent voltage positive peak duration time and maximum positive voltage.

(Fig. S5a). A high-speed video camera was adopted to capture the destruction processes and record the residual velocities. The voltage signals were acquired by a digital oscilloscope.

Firstly, a wearable suit based on EK-TENG was tailored and worn on a model to study its safeguarding properties under the high-speed ballistic impact (Fig. 5a). In comparison, a Kevlar-based suit was also applied. The shooting speeds of bullets on neat Kevlar and EK-TENG were 151.5 m/s and 153.8 m/s, respectively. Interestingly, the toy wearing Kevlar-suit was completely penetrated which led to serious hurt. On the contrary, the bullet was effectively blocked by the EK-TENG based suit (Video S1). This proved the as-prepared EK-TENG could impede the high-speed shooting damage.

Supplementary material Video S1 can be found online at doi:10.1016/j.nanoen.2021.106657.

Furthermore, the fabrics (area of 85 × 85 mm^2) were fixed on a steel frame for systematic testing. The high-speed photography photos of Kevlar and EK-TENG under the incident velocity of 160 m/s were shown in Fig. 5b and Video S2. A longer bullet breakdown time and greater deformation of EK-TENG were observed than Kevlar. Additionally, Fig. 5c illustrated the residual velocities (v_r) of bullets at different incident velocities (v_i). The relationship between them was fitted by the Recht-Ipson function [32]:

$$v_r = \alpha(v_i^p - v_{bl}^p)^{1/p} \tag{1}$$

Where α and p were the parameters controlling the shape of the curve, v_{bl} was the ballistic limit velocity. When the fabric could not be penetrated, v_r was considered to be 0. The fitting results were shown in solid lines. It was clear that the function fitted well with the experimental results. The v_{bl} of EK-TENG was 126.6 m/s, which was higher than 90.1 m/s of neat Kevlar. Moreover, the relationship between the dissipated energy (E_{dis}) and the incident energy (E_i) was shown in Fig. S5b–d. The dissipated energy was calculated via formula (2) as followed:

$$E_{dis} = \frac{1}{2}mv_i^2 - \frac{1}{2}mv_r^2 \tag{2}$$

Where m was the mass of the bullet. In particular, at the identical incident velocities, such as 138 m/s or 160 m/s (Fig. 5d), the energy dissipation ratios of EK-TENG were larger than neat Kevlar. Accordingly, the EK-TENG could dissipate more energy compared with neat Kevlar, confirming its high-speed protection properties.

Supplementary material Video S2 can be found online at doi:10.1016/j.nanoen.2021.106657.

Moreover, a finite element model was established to verify the enhanced ballistic performance of EK-TENG. The simulated impact processes of neat Kevlar and EK-TENG at the same incident velocity were presented in Fig. S6. Larger fabric deformation and a smaller bullet residual velocity of EK-TENG was observed than Kevlar. The impact stress cloud diagram of EK-TENG under the condition of fully fixed support was shown in Fig. S7. It was found that the stress in the yarn increased with time and the stress wave propagated from the center to the boundary in a symmetrical form. The fabric was deformed after being impacted, and the fabric was broken when the time was 60 μs.

In addition, the self-powered sensing performance of EK-TENG under high-speed impact was evaluated. The voltage signals of EK-TENG at the shooting velocities of 82.3 m/s, 125.8 m/s and 183.5 m/s were presented in Fig. 5e. It could be observed that the increase in ballistic impact velocities resulted in an improvement in peak voltages while the duration time of positive voltage (T_{up}) also showed a substantial decrement. Meanwhile, T_{up} exhibited a decreasing tendency from 746.8 μs to 44.2 μs in shooting speeds of 60–150 m/s and finally saturated after 150 m/s loading (Fig. 5f). This result indicated T_{up} values could be used to assess external shooting speeds EK-TENG suffered. For instance, when the T_{up} was 402 μs, the initial speed of bullet was 76 m/s while 204 μs was corresponded to 94 m/s. The numerical calculations of the electric potential distribution of EK-TENG during impact were shown in Fig. S8. As the bullet approached, the electric potential of EK-TENG gradually decreased along with the distribution became uneven due to the local influence increased.

2.5. EK-TENG protection and sensing characteristics under explosion damage

Besides, the anti-shockwave performance of EK-TENG subjected to air blast was further investigated. Fig. 6a schematically demonstrated the explosion test system. To generate a shock wave, an explosive charge composed of Pentaerythrite Tetranitrate with a mass of 1 g was fixed at the center of the 304 stainless steel plate (300 × 300 × 1.5 mm^3) with a blast distance (h_0) of 5 mm, 10 mm and 15 mm, respectively. The photographs of the device on top and side view were shown in Fig. S9a. The EK-TENG was attached to the bottom surface of 304 stainless steel plate. Also, the strain rates loaded on the composite plates were measured by the strain gauge which was connected with a bridge box and a dynamic strain gauge. The pressure-time history of the transmitted shock wave was measured by the piezoelectric film (a PVDF pressure gauge) mounted on the midpoint of the base. Ultimately, the voltage signals of EK-TENG were directly collected by an oscilloscope.

The pressure-time history of the incident shock wave (P_0, unit: MPa) was calculated by formulas as followed [33,34] and shown in Fig. 6b:

$$P_0 = P_m \bullet \exp[f_0](-\frac{t}{\theta}) \tag{3}$$

$$P_m = 100 \bullet (\frac{r}{r_0})^{-1.38} \tag{4}$$

$$\theta = 10^{-6} \bullet (\frac{r}{r_0})^{1.6} \tag{5}$$

Among them, P_m (unit: MPa) was the maximum value of the pressure at the measured wavefront; t (unit: s) was the time since the explosion started and the θ (unit: s) was the reference time; r_0 (unit: mm) was the charge radius of 0.2 mm and r (unit: mm) was the distance from test point to explosive center which was the sum of h_0 and r_0. Clearly, a slight decrement in h_0 resulted in the significant enhancement of P_m.

Furthermore, the results of strain rate at different blast distances were shown in Fig. S9b. All measured values were between 11.2 × 10^6 s^{-1} and 12.6 × 10^6 s^{-1}. After the explosion, large deformations were generated in the 304 stainless steel plates. The pure steel plate was severely damaged after the explosion (Fig. S9c (i)), and many fragments were produced, which was also dangerous for human body. However, the surface of the steel plate with EK-TENG attachment was intact even the strain gauge was still stuck to the plate (Fig. S9c (ii)).

More importantly, the excellent shockwave attenuation performance of EK-TENG was characterized by measuring transmitted waves at different explosion heights. Under blast loading of 5 mm (Fig. 6c), the transmission wave pressure (P) of the 304 stainless steel plate reached a peak value of 6.4 MPa at 152.6 μs, while the transmission wave peak pressure of the composite plate with a single-layer Kevlar was 1.8 MPa, attenuated by 72.8%. Notably, the transmission wave peak pressure of the plate with a single-layer EK-TENG was 0.8 MPa, attenuated by 87.4%. Meanwhile, similar enhanced energy-dissipation effect of EK-TENG could be found in Fig. S9d and Fig. S9e. In addition, the decay time of the transmitted wave was prolonged due to the introduction of EK-TENG, which impeded and dissipated the concentrated loading of ultra-high stress waves. Peak value comparison of the transmitted waves pressure (P_{max}) was illustrated in Fig. 6d. It could be concluded that EK-TENG demonstrated more excellent energy absorption performance than neat Kevlar.

Finally, Fig. S9f displayed the test loading method of electric signal under explosion damage and the contact material was Poly tetra fluoroethylene. The negative peak time difference of the voltage signal was defined as t_0, and the values of t_0 at three heights were counted. As the explosion height increased, an increment in t_0 was observed in Fig. 6e.

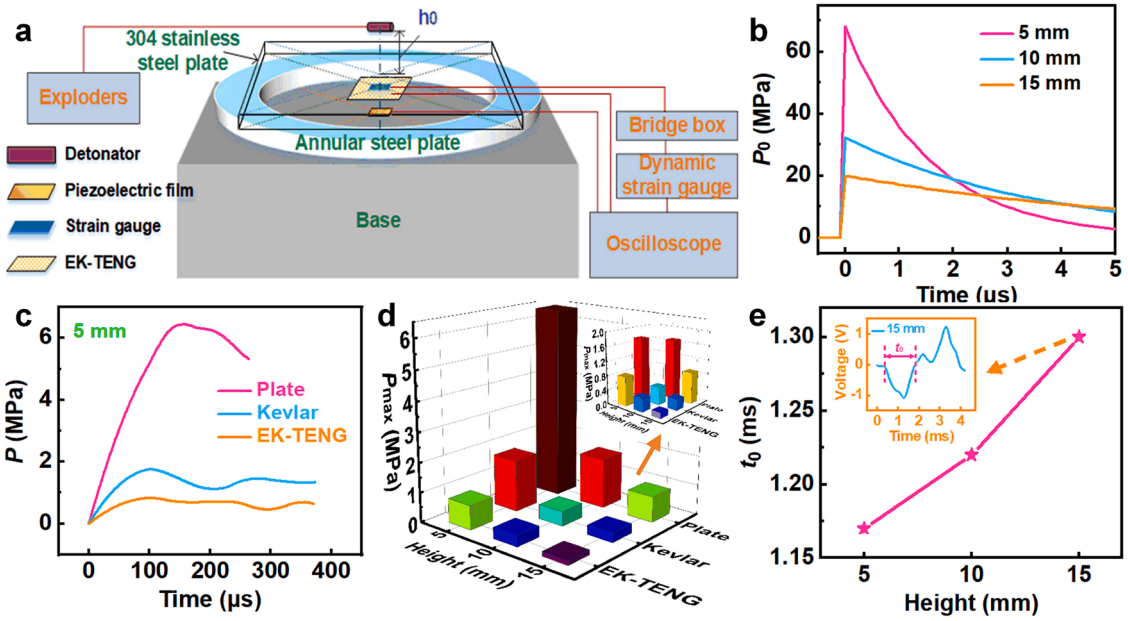

Fig. 6. (a) Schematic of the explosion test system. (b) Pressure-time history of explosion incident waves at different explosion heights. (c) Pressure-time history of transmitted waves at explosion height of 5 mm. (d) Explosion height dependent pressures of transmitted waves of various fabrics. (e) The sensing signals generated by EK-TENG under explosion.

For instance, when the explosion distance was 15 mm, the stable voltage signal of EK-TENG was shown in the insert figure. Overall, EK-TENG not only showed excellent anti-shockwave performance, but also could be used in the field of ultra-hazard sensing.

2.6. *The application of EK-TENG wireless passive sensor alarm*

Besides excellent protection and superior self-powered electrical performance, transmitting the sensing signals to readable electrical devices and alarm human beings were vital in automatic security applications. EK-TENG, as a wearable self-powered device, may also work in many complex conditions with low, medium and even high-speed force loadings. Finding the broken EK-TENGs after impact was important for replacing them and rescuing in time. Hence an intelligent wireless passive alarm system based on EK-TENG with human motion monitoring and impact sensing effects for remote emergency rescue was finally developed. Three typical loading modes with different frequencies such as low-velocity human walking motion (Mode I), medium-velocity drop hammer impact (Mode II) and high-velocity bullet impact (Mode III) were carried out to generate voltage signals (Fig. S10).

The as-developed alarming system was shown in Fig. 7a. Briefly, the signals generated by EK-TENG were firstly filtered and amplified by the signals processing circuits (SP circuits) and subsequently transformed by an analog to digital converter (ADC), finally accepted and analyzed by a microcontroller. In addition, the microcontroller unit (MCU) had a visual screen (Fig. 7b), which could not only dynamically display the detected waveforms but also conveniently set the threshold of the internal program and the alarm switch whether to turn on in a friendly human-computer interaction. A custom smartphone application was developed and programmed. When the MCU detected a danger, the electrical signals were transmitted wirelessly to a smartphone by Bluetooth communication. The dialog box would pop up to prompt the "Alarm" on the application program interface, as displayed in Fig. 7c.

When the signals were transmitted to the microcontroller, the peak values and time difference of the voltage signals were firstly detected. The absolute value of the peak voltage ($|U|$) and the time difference between the peak-to-peak values ($|\Delta t|$) were used as the two main parameters for judging the danger signals. The flow chart of the EK-TENG wireless passive sensor alarm was demonstrated in Fig. 7d. Here, the requirement of $|U| \geq U_1$ could eliminate the influence of noise and error interference in the signal. But the $|\Delta t|$ was the main factor in deciding whether to send an alarm signal to smartphone by Bluetooth. In general, the $|\Delta t|$ values of three loading modes were all less than 200 ms. As illustrated in Fig. 7e, the $|\Delta t|$ of voltage generated by normal walking was greater than 50 ms and $|\Delta t|$ of the drop hammer impact was between 2 ms and 50 ms. However, the $|\Delta t|$ of bullet impact was less than 2 ms. Consequently, based on the above analysis, different alarm responses were generated by setting different judgment thresholds. For instance, when the judgment threshold of $|\Delta t|$ (Δt_1) was set to 200 ms, the walking signal not only trigger the MCU to sound, but also prompted a warning on the mobile phone interface through Bluetooth (Fig. 7f). But when the Δt_1 was set to 50 ms, no alarm occurred during human walking process (Fig. S11a). Similarly, there was an alarm at the Δt_1 of 50 ms (Fig. 7g) whereas no alarm at the Δt_1 of 2 ms (Fig. S11b) under the EK-TENG suffering drop hammer impact. Finally, EK-TENG sent out an alarm through the wireless system under the shooting of high-speed bullet, warning the impact danger and prompting the remote monitor to initiate a rescue (Fig. 7h). The detailed alarm process was shown in Video S3. Therefore, this wireless sensing system based on the EK-TENG showed high sensitivity to various excitations and could be used to monitor and warn impact dangers to meet different practical requirements which demonstrated potential application in safeguarding and smart electronics.

Supplementary material Video S3 can be found online at doi:10.1016/j.nanoen.2021.106657.

3. Conclusion

In summary, we had successfully manufactured a flexible and wearable enhanced Kevlar-based triboelectric nanogenerator, which not only showed anti-impact and self-powered sensing performance but also could be used for smart wireless security alarm applications. The fabricated EK-TENG could deliver the maximum peak power density of 25.8 mW/m^2 at the matching impedances of 10 MΩ. It was capable of directly powering commercial LEDs and supercapacitors, showing good triboelectric and energy harvesting performance. EK-TENG also exhibited excellent stability of repeated contact-separation loadings over 1000 cycles. In addition, the maximum pull-out force of EK-TENG

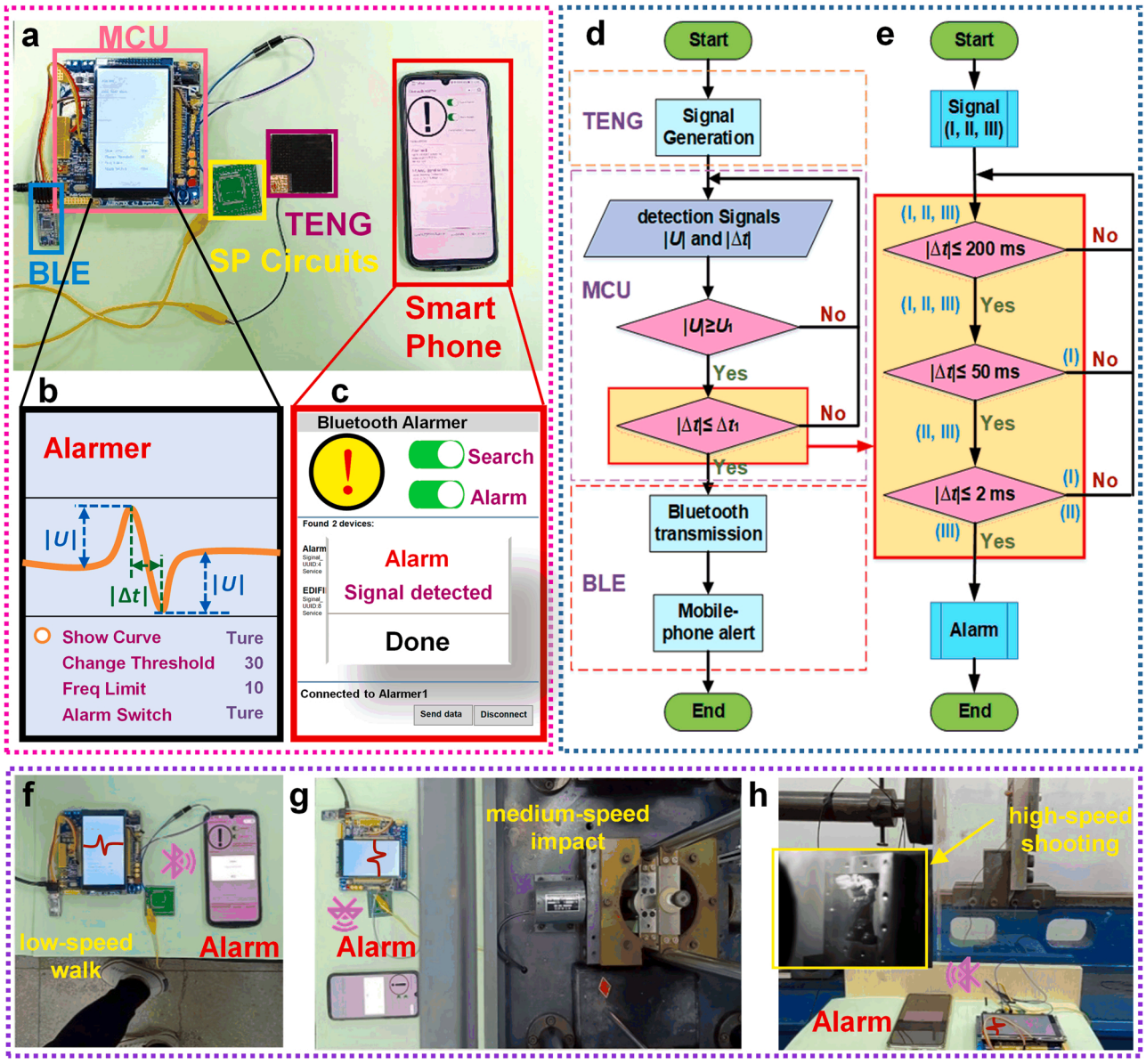

Fig. 7. (a) The sensing system contained TENG-based Bluetooth and the interface of (b) microcontroller and (c) smartphone. (d) The flow chart of TENG wireless passive sensor alarm. (e) Alarm results of three loading modes under different set thresholds. The sensor system sensed, transmitted and warned during the impact of (f) low-speed, (g) medium-speed and (h) high-speed.

was about 14 times as large as neat Kevlar at the pull-out velocity of 5 mm/s, suggesting that the friction between yarns increased due to the introduction of STF and SSG. Moreover, EK-TENG presented the significant safeguarding and energy-absorbing performance which EK-TENG dissipated 77.9% hammer impact force at a falling height of 100 mm. Besides, EK-TENG effectively resisted a shooting speed of 126.6 m/s and dissipated 87.4% of the explosion wave under blast loading. Meanwhile, EK-TENG could stably output voltage signals even at high frequency and high strain rate impact. Ultimately, a smart TENG-based wireless passive sensor alarm system was demonstrated to verify EK-TENG's superior sensing sensitivity and application of monitoring and warning impact dangers. In conclusion, the as-designed EK-TENG as well as wireless passive sensor alarm system with enhanced anti-impact and energy-harvesting performance showed profound application in human motion monitoring, remote emergency rescue and automated security system.

4. Experiment section

4.1. Materials

All chemical reagents were of analytical purity and used as received without further purification. Hydroxyl silicone oil, boric acid, ethanol and polyethylene glycol (PEG200) were provided by Sinopharm Chemical Reagent Co. Ltd, Shanghai, China. The spherical silica particles were purchased from Shanghai Bu Micro Applied Materials Technology Co., Ltd. The few-layer graphene was supplied by Shenzhen Siheng Technology Co., Ltd, China. The plain-woven aramid Kevlar fabric with an areal density of 200 g/m^2 was bought from Beijing Junantai Protection Technology Co., Ltd., China.

4.2. Preparation procedures

4.2.1. Preparation of STF

The spherical silica particles were added into PEG200 and dispersed

by ball milling for 24 h at room temperature to prepare STF with different mass fractions.

4.2.2. Preparation of Kevlar/STF

The Kevlar/STF composite was prepared by a "drip and dry" method. Firstly, STF was diluted with ethanol at a volume ratio of 1:4 and then mixed for 30 min in ultra-sonication to obtain a homogeneous solution. Subsequently, Kevlar fabric was immersed in the diluted solution for 1 min and then were placed in an oven at 80 ℃ for 6 h to evaporate the ethanol. The Kevlar/STF composites were obtained.

4.2.3. Preparation of SSG

Briefly, hydroxyl silicone oil and boric acid with a mass ratio of 30:1 were thoroughly mixed. And the mixture solution was heated in an oven for 1 h. Then, octanoic acid was added to the mixture and vigorously stirred. The composite was heated for another 30 min and cooled to room temperature to obtain SSG.

4.2.4. The fabrication procedures of EK-TENG

A certain amount of graphene was dispersed in ethanol. Then, the Kevlar/STF composites, which were obtained by a "drip and dry" method, were hung vertically and the mixed graphene solution was dripped on the surface. After placing in an 80 °C oven to evaporate the organic solvents, G-Kevlar/STF was obtained. Then, a conductive wire was placed on the surface of graphene. Meanwhile, another solution of SSG and ethanol was also prepared. Due to the viscosity of SSG, the SSG-film was adhered on the surface of G-Kevlar/STF after the ethanol evaporated, and the graphene was wrapped inside. Finally, they were placed in an oven at 80 ℃ to obtain the EK-TENG.

4.3. Characterization

The micro-morphology of all composites were characterized by field emission scanning electron microscopy (SEM, Gemini 500, Carl Zeiss Jena, Germany). Rheological properties of the STFs were tested by a commercial rheometer (Physica MCR 302, Anton Paar Co., Austria) with cone-plate geometry (25 mm in diameter and 2° in cone angle) under steady shear. The storage modulus and loss modulus of the SSG were also measured using Physica MCR 302. The composites, molded into a cylinder shape with a thickness of 0.85 mm and diameter of 20 mm, were tested with a parallel plate (diameter of 20 mm). The triboelectric properties of EK-TENG were investigated by an oscillator (JZK-10) (bought from Sinocera Piezotronics INC, China) and the corresponding output signals were recorded using a digital multimeter (DMM 6001). To study the interaction between yarns in fabric, yarn pull-out tests were carried out using a universal tensile instrument (MTS, Criterion™ Model 43). The energy-collecting and safeguarding properties of the EK-TENG were performed by a low-velocity drop hammer test device and high-speed ballistic impact experiment. Finally, the explosion test system was used to study the anti-shockwave performance of EK-TENG.

CRediT authorship contribution statement

Wenhui Wang: Methodology, Software, Writing – original draft preparation. **Jianyu Zhou:** Data curation, Validation, **Sheng Wang:** Conceptualization, Writing – review & editing, **Fang Yuan:** Visualization, Investigation. **Shuai Liu:** Visualization, Software. **Junshuo Zhang:** Formal analysis. **Xinglong Gong:** Supervision, Funding acquisition.

Declaration of Competing Interest

The authors declare that they have no known competing financial interests or personal relationships that could have appeared to influence the work reported in this paper.

Acknowledgment

Financial supports from the National Natural Science Foundation of China (Grant No. 11972032, 11802303, 11772320, 12132016, 12172349), USTC Research Funds of the Double First-Class Initiative (YD2480002004) and the Fundamental Research Funds for the Central Universities (WK2480000009) are gratefully acknowledged.

Appendix A. Supporting information

Supplementary data associated with this article can be found in the online version at doi:10.1016/j.nanoen.2021.106657.

References

[1] J. Xiong, J. Chen, P.S. Lee, Functional fibers and fabrics for soft robotics, wearables, and human-robot interface, Adv. Mater. 33 (2021), 098302, https://doi.org/10.1002/adma.202002640.
[2] K.J. Baeg, J. Lee, Flexible electronic systems on plastic substrates and textiles for smart wearable technologies, Adv. Mater. Technol. 5 (2020), 2000071, https://doi.org/10.1002/admt.202000071.
[3] W. Ma, Y. Zhang, S. Pan, Y. Cheng, Z. Shao, H. Xiang, G. Chen, L. Zhu, W. Weng, H. Bai, M. Zhu, Smart fibers for energy conversion and storage, Chem. Soc. Rev. 50 (2021) 7009–7061, https://doi.org/10.1039/d0cs01603a.
[4] T. Bhatta, P. Maharjan, H. Cho, C. Park, S.H. Yoon, S. Sharma, M. Salauddin, M. T. Rahman, S.M.S. Rana, J.Y. Park, High-performance triboelectric nanogenerator based on MXene functionalized polyvinylidene fluoride composite nanofibers, Nano Energy 81 (2021), 105670, https://doi.org/10.1016/j.nanoen.2020.105670.
[5] K.M. Shi, H.Y. Zou, B. Sun, P.K. Jiang, J.L. He, X.Y. Huang, Dielectric modulated cellulose paper/PDMS-based triboelectric nanogenerators for wireless transmission and electropolymerization applications, Adv. Funct. Mater. 30 (2020), 1904536, https://doi.org/10.1002/adfm.201904536.
[6] J.L. Wang, X. Yu, D. Zhao, Y. Yu, Q. Gao, T.H. Cheng, Z.L. Wang, Enhancing output performance of triboelectric nanogenerator via charge clamping, Adv. Energy Mater. 11 (2021), 2101356, https://doi.org/10.1002/aenm.202101356.
[7] G. Zhu, B. Peng, J. Chen, Q.S. Jing, Z.L. Wang, Triboelectric nanogenerators as a new energy technology: From fundamentals, devices, to applications, Nano Energy 14 (2015) 126–138, https://doi.org/10.1016/j.nanoen.2014.11.050.
[8] K. Dong, X. Peng, J. An, A.C. Wang, J.J. Luo, B.Z. Sun, J. Wang, Z.L. Wang, Shape adaptable and highly resilient 3D braided triboelectric nanogenerators as E-textiles for power and sensing, Nat. Commun. 11 (2020) 2868–2879, https://doi.org/10.1038/s41467-020-16642-6.
[9] Y.C. Lai, H.W. Lu, H.M. Wu, D.G. Zhang, J.Y. Yang, J. Ma, M.; Shamsi, V.; Vallem, M.D. Dickey, Elastic multifunctional liquid-metal fibers for harvesting mechanical and electromagnetic energy and as self-powered sensors, Adv. Energy Mater. 11 (2021), 2100411, https://doi.org/10.1002/aenm.202100411.
[10] C.X. Wu, T.W. Kim, F.S. Li, T.L. Guo, Wearable electricity generators fabricated utilizing transparent electronic textiles based on polyester/Ag nanowires/graphene core-shell nanocomposites, ACS Nano 10 (2016) 6449–6457, https://doi.org/10.1021/acsnano.5b08137.
[11] W. Paosangthong, R. Torah, S. Beeby, Recent progress on textile-based triboelectric nanogenerators, Nano Energy 55 (2019) 401–423, https://doi.org/10.1016/j.nanoen.2018.10.036.
[12] S.S. Kwak, H.J. Yoon, S.W. Kim, Textile-based triboelectric nanogenerators for self-powered wearable electronics, Adv. Funct. Mater. 29 (2019), 1804533, https://doi.org/10.1002/adfm.201804533.
[13] Y. Zhao, X. Li, J.N. Shen, C.J. Gao, B. van der Bruggen, The potential of kevlar aramid nanofiber composite membranes, J. Mater. Chem. A 8 (2020) 7548–7568, https://doi.org/10.1039/d0ta01654c.
[14] S.S. Cao, H.M. Pang, C.Y. Zhao, S.H. Xuan, X.L. Gong, The CNT/PSt-EA/kevlar composite with excellent ballistic performance, Compos. B. Eng. 185 (2020), 107793, https://doi.org/10.1016/j.compositesb.2020.107793.
[15] J.B. Qin, B.R. Guo, L. Zhang, T.W. Wang, G.C. Zhang, X.T. Shi, Soft armor materials constructed with kevlar fabric and a novel shear thickening fluid, Compos. B. Eng. 183 (2020), 107686, https://doi.org/10.1016/j.compositesb.2019.107686.
[16] H. Wang, H. Wang, Y. Wang, X. Su, C. Wang, M. Zhang, M. Jian, K. Xia, X. Liang, H. Lu, S. Li, Y. Zhang, Laser writing of janus graphene/kevlar textile for intelligent protective clothing, ACS Nano 14 (2020) 3219–3226, https://doi.org/10.1021/acsnano.9b08638.
[17] A. Hazarika, B.K. Deka, C. Jeong, Y.B. Park, H.W. Park, Biomechanical energy-harvesting wearable textile-based personal thermal management device containing epitaxially grown aligned Ag-Tipped-NixCo1-xSe nanowires/reduced graphene oxide, Adv. Funct. Mater. 29 (2019), 1903144, https://doi.org/10.1002/adfm.201903144.
[18] L.X. Ma, J.W. Zhang, C.Q. Teng, Covalent functionalization of aramid fibers with zinc oxide nano-interphase for improved UV resistance and interfacial strength in composites, Compos. Sci. Technol. 188 (2020), 107996, https://doi.org/10.1016/j.compscitech.2020.107996.
[19] C.V. Moraes, V.D. da Silva, M.V. Castegnaro, J. Morais, H.S. Schrekker, S.C. Amico, Lightweight composites through imidazolium ionic liquid enhanced aramid-epoxy resin interactions, ACS Appl. Polym. Mater. 2 (2020) 1754–1763, https://doi.org/10.1021/acsapm.9b01145.

[20] A. Srivastava, A. Majumdar, B.S. Butola, Improving the impact resistance of textile structures by using shear thickening fluids: a review, Crit. Rev. Solid State Mater. Sci. 37 (2012) 115–129, https://doi.org/10.1080/10408436.2011.613493.
[21] C.Y. Zhao, X.L. Gong, S. Wang, W.Q. Jiang, S.H. Xuan, Shear stiffening gels for intelligent anti-impact applications, Cell Rep. Phys. Sci. 1 (2020), 100266, https://doi.org/10.1016/j.xcrp.2020.100266.
[22] E. Brown, H.M. Jaeger, Shear thickening in concentrated suspensions: phenomenology, mechanisms and relations to jamming, Rep. Prog. Phys. 77 (2014), 046602, https://doi.org/10.1088/0034-4885/77/4/046602.
[23] S. Gurgen, M.C. Kushan, W.H. Li, Shear thickening fluids in protective applications: a review, Prog. Polym. Sci. 75 (2017) 48–72, https://doi.org/10.1016/j.progpolymsci.2017.07.003.
[24] U. Mawkhlieng, A. Majumdar, Deconstructing the role of shear thickening fluid in enhancing the impact resistance of high-performance fabrics, Compos. B. Eng. 175 (2019), 107167, https://doi.org/10.1016/j.compositesb.2019.107167.
[25] S. Gurgen, M.C. Kushan, W.H. Li, Shear thickening fluids in protective applications: a review, Prog. Polym. Sci. 75 (2017) 48–72, https://doi.org/10.1016/j.progpolymsci.2017.07.003.
[26] L. Liu, M. Cai, X. Liu, Z. Zhao, W. Chen, Ballistic impact performance of multi-phase STF-impregnated Kevlar fabrics in aero-engine containment, Thin Wall Struct. 157 (2020), 107103, https://doi.org/10.1016/j.tws.2020.107103.
[27] J. Qin, B. Guo, L. Zhang, T. Wang, G. Zhang, X. Shi, Soft armor materials constructed with Kevlar fabric and a novel shear thickening fluid, Compos. B. Eng. 183 (2020), 107686, https://doi.org/10.1016/j.compositesb.2019.107686.
[28] S. Wang, S.H. Xuan, W.Q. Jiang, W.F. Jiang, L.X. Yan, Y. Mao, M. Liu, X.L. Gong, Rate-dependent and self-healing conductive shear stiffening nanocomposite: a novel safe-guarding material with force sensitivity, J. Mater. Chem. A 3 (2015) 19790–19799, https://doi.org/10.1039/c5ta06169e.
[29] Y.P. Wang, S. Wang, C.H. Xu, S.H. Xuan, W.Q. Jiang, X.L. Gong, Dynamic behavior of magnetically responsive shear-stiffening gel under high strain rate, Compos. Sci. Technol. 127 (2016) 169–176, https://doi.org/10.1016/j.compscitech.2016.03.009.
[30] S.S. Zhang, S. Wang, T. Hu, S.H. Xuan, H. Jiang, X.L. Gong, Study the safeguarding performance of shear thickening gel by the mechanoluminescence method, Compos. B. Eng. 180 (2020), 107564, https://doi.org/10.1016/j.compositesb.2019.107564.
[31] S. Wang, S. Xuan, M. Liu, L. Bai, S. Zhang, M. Sang, W. Jiang, X. Gong, Smart wearable Kevlar-based safeguarding electronic textile with excellent sensing performance, Soft Matter 13 (2017) 2483–2491, https://doi.org/10.1039/c7sm00095b.
[32] R.F. Recht, T.W. Ipson, Ballistic perforation dynamics, J. Appl. Mech. 30 (1963) 384–390, https://doi.org/10.1115/1.3636566.
[33] Q. Liu, Y.L. Duan, H.H. Ma, X.P. Long, Y. Han, Review on the exploration of condensed carbon formation mechanism in detonation products, AIP Adv. 10 (2020) 050701–050714, https://doi.org/10.1063/1.5142521.
[34] L.J. Ren, H.H. Ma, Z.W. Shen, Y.X. Wang, K. Zhao, Blast resistance of water-backed metallic sandwich panels subjected to underwater explosion, Int. J. Impact Eng. 129 (2019) 1–11, https://doi.org/10.1016/j.ijimpeng.2019.02.009.